Chapter 1

Introduction

1.1 Spontaneous emission in vacuum

A two-level atom that is initially in its excited state will, at some time later, spontaneously decay to its ground state with a lower energy and simultaneously emit a photon. The instant of this transition is random and therefore a probability per unit time or transition rate (also called decay rate or spontaneous emission rate) is introduced to describe this stochastic behavior. The transition rate of an excited atom can be studied by repeating the measurement of transition events on a single atom, or by measuring an ensemble of identical and independent atoms. Theoretically, this seemingly simple "spontaneous" emission, however, can not be explained by a semiclassical theory in which the atomic system is quantized and the radiation field is treated classically, because in that case an excited atom in vacuum will never decay. This problem can only be solved in quantum electrodynamics (QED) in which electromagnetic fields are quantized leading to a concept of vacuum field or vacuum photon (virtual photon) that even exists in "vacuum" without actual photons. It is the vacuum field that perturbs the atom causing the "spontaneous" emission. The "spontaneous" emission can be thought of as "stimulated" emission by interacting with virtual photons. In this section, we will study the spontaneous emission in vacuum in the framework of QED. This topic has been covered by many textbooks such as [10, 11, 12].

In quantum mechanics, the transition rate from an initial state $|i\rangle$ to a final state $|j\rangle$ under an interaction Hamiltonian H' by using the first-order perturbation theory can be written as

$$w_{ij} = \frac{2\pi}{\hbar}|\langle i|H'|j\rangle|^2\delta(E_i - E_j), \tag{1.1}$$

where the Hamiltonian of the system is $H = H_0 + H'$ with H_0 being the unperturbed Hamiltonian and H' is treated as a perturbation, $|i\rangle$ and $|j\rangle$ are

the eigenstates of H_0 with the corresponding eigenenergies of E_i and E_j, and $\hbar$ is reduced Planck's constant. For the perturbation theory to be valid, H' should be small compared with H_0 and the eigenstates and eigenenergies of H do not differ much from those of H_0. Here the term $\delta(E_i - E_j)$ ensures energy conservation during the transition.

We apply Eq. (1.1) to spontaneous emission of a two-level atom in vacuum. The states are given by

$$|i\rangle = |e, 0\rangle_{\boldsymbol{k},l} \equiv |e\rangle \otimes |0\rangle_{\boldsymbol{k},l} \text{ and } |j\rangle = |g, 1\rangle_{\boldsymbol{k}',l'} \equiv |g\rangle \otimes |1\rangle_{\boldsymbol{k}',l'}, \tag{1.2}$$

where "e" ("g") denotes the excited (ground) state of the atom, "0" and "1" indicate the number of photons, and $\boldsymbol{k}$ and $l = 1, 2$ ($\boldsymbol{k}'$ and l') are the wave vector and polarization label of the initial (final) photon state, respectively. The interaction Hamiltonian reads

$$H' = -\boldsymbol{\mu} \cdot \boldsymbol{E}, \tag{1.3}$$

where $\boldsymbol{\mu}$ is the operator of the atomic dipole moment, $\boldsymbol{E}$ is the operator of the electric field, and we have used the dipole approximation assuming the transition wavelength is much larger than the dimension of the atomic wavefunction. According to the theory of QED, an electromagnetic wave as a function of position $\boldsymbol{r}$ and time t can be quantized on a planar wave basis:

$$\boldsymbol{E}(\boldsymbol{r}, t) = i \sum_{l=1,2} \sum_{\boldsymbol{k}} \hat{\boldsymbol{e}}_{\boldsymbol{k},l} \sqrt{\frac{\hbar \omega_k N_{\boldsymbol{k},l}}{2\epsilon_0 V}} \left[a_{\boldsymbol{k},\boldsymbol{l}} e^{i(\boldsymbol{k}\cdot\boldsymbol{r} - \omega_k t)} - a^\dagger_{\boldsymbol{k},\boldsymbol{l}} e^{-i(\boldsymbol{k}\cdot\boldsymbol{r} - \omega_k t)} \right], \tag{1.4}$$

where $\hat{\boldsymbol{e}}_{\boldsymbol{k},l}$ is a unit polarization vector, orthogonal to $\boldsymbol{k}$, $N_{\boldsymbol{k},l}$ is the number of photons, $\omega_k = ck$ is the angular frequency corresponding to a wave number $k = |\boldsymbol{k}|$ with c being the speed of light in vacuum, ϵ_0 is the vacuum permittivity, V is a quantization volume, $a_{\boldsymbol{k},\boldsymbol{l}}$ ($a^\dagger_{\boldsymbol{k},\boldsymbol{l}}$) is the annihilation (creation) operator.

By plugging Eqs. (1.2), (1.3), and (1.4) into Eq. (1.1), we obtain the transition rate for specific $\boldsymbol{k}$ and l of the final photon state:

$$w(\boldsymbol{k}, l) = \frac{N_{\boldsymbol{k},l} \pi \omega_{\boldsymbol{k}}}{\hbar \epsilon_0 V} \left| \hat{\boldsymbol{e}}_{\boldsymbol{k},l} \cdot \hat{\boldsymbol{z}} \right|^2 \mu^2 \delta(\omega_{\boldsymbol{k}} - \omega_0), \tag{1.5}$$

where $\hat{\boldsymbol{z}}$ is a unit vector parallel with $\boldsymbol{\mu}$, $\mu = |\langle e|\boldsymbol{\mu}|g\rangle|$, and ω_0 is the resonance frequency of the atom. Here we have used the following properties of the annihilation and creation operators as well as the photon number states:

$$a_{\boldsymbol{k},l}|n\rangle_{\boldsymbol{k},l} = \sqrt{n}|n-1\rangle_{\boldsymbol{k},l}, \; a^\dagger_{\boldsymbol{k},l}|n\rangle_{\boldsymbol{k},l} = \sqrt{n+1}|n+1\rangle_{\boldsymbol{k},l},$$
$$_{\boldsymbol{k},l}\langle n|n\rangle_{\boldsymbol{k},l} = 1, \tag{1.6}$$

In the theory of QED, we have $N_{\boldsymbol{k},l} = 1/2$ for the vacuum state. However, it has been proven that this one-half vacuum photon contributes only half of the spontaneous emission rate and that another half of the spontaneous emission rate stems from radiation reaction. The fact that the vacuum photon alone can not induce spontaneous emission explains why spontaneous absorption never happens by the interaction with the vacuum photon—the vacuum photon and radiation reaction cancel with each other in this case. Detailed discussions on the vacuum photon and radiation reaction are beyond the scope of this thesis and to this end we set $N_{\boldsymbol{k},l} = 1$ to include the effect of radiation reaction (see Ref. [13] for a detailed discussion on this topic).

For spontaneous emission in vacuum, the final photon state has no preferable $\boldsymbol{k}$ or l and we need to integrate over all $\boldsymbol{k}$ and l in Eq. (1.5) to obtain the spontaneous emission rate:

$$\begin{aligned} w &= \frac{2V}{8\pi^3}\int_{-\infty}^{\infty} \mathrm{d}\boldsymbol{k}\, w(\boldsymbol{k},l) \\ &= \frac{2V}{8\pi^3}\int_0^{2\pi}\mathrm{d}\phi\int_0^{\pi}\sin\theta\,\mathrm{d}\theta\int_0^{\infty}\frac{\omega_{\boldsymbol{k}}^2}{c^3}\,\mathrm{d}\omega_{\boldsymbol{k}}\, w(\boldsymbol{k},l) \\ &= \frac{\mu^2\omega_0^3}{3\pi\epsilon_0\hbar c^3}, \end{aligned} \tag{1.7}$$

where "2" in the nominator of the pre-factor before the integral accounts for the two polarization states and the term $V/8\pi^3$ is the number of modes in a unit volume in k-space.

1.2 Spontaneous emission in a uniform medium

We will continue our discussion with the situation in which the atom is located in an infinite and uniform medium with a phase refractive index n_p. In general, the medium is dispersive with a group refractive index n_g. Equations (1.1)–(1.3) remain the same, but Eqs. (1.4) and (1.5) are modified as

$$\boldsymbol{E}(\boldsymbol{r},t) = i\sum_{l=1,2}\sum_{\boldsymbol{k}}\hat{\boldsymbol{e}}_{\boldsymbol{k},l}\sqrt{\frac{N_{\boldsymbol{k},l}\hbar\omega_k}{2n_p n_g\epsilon_0 V}}\left[a_{\boldsymbol{k},\boldsymbol{l}}e^{i(\boldsymbol{k}\cdot\boldsymbol{r}-\omega_k t)} - a^{\dagger}_{\boldsymbol{k},\boldsymbol{l}}e^{-i(\boldsymbol{k}\cdot\boldsymbol{r}-\omega_k t)}\right], \tag{1.8}$$

and

$$w(\boldsymbol{k},l) = \frac{N_{\boldsymbol{k},l}\pi\omega_{\boldsymbol{k}}}{n_p n_g\hbar\epsilon_0 V}\left|\hat{\boldsymbol{e}}_{\boldsymbol{k},l}\cdot\hat{\boldsymbol{z}}\right|^2\mu^2\delta(\omega_{\boldsymbol{k}}-\omega_0). \tag{1.9}$$

The density of modes is also changed and therefore Eq. (1.7) becomes

$$w = \frac{2n_p^2 n_g V}{8\pi^3}\int_0^{\infty}\mathrm{d}\boldsymbol{k}\, w(\boldsymbol{k},l) = \frac{n_p\mu^2\omega_0^3}{3\pi\epsilon_0\hbar c^3}. \tag{1.10}$$

We notice that compared with vacuum an infinite and uniform material with a phase refractive index n_p increases the spontaneous emission rate by a factor of n_p and that the group refractive index cancels out and does not appear in the expression of the spontaneous emission rate [14].

1.3 Cavity quantum electrodynamics

A cavity is a resonant optical element which stores light for a certain lifetime. The electromagnetic field in a cavity is enhanced as well as the vacuum field. As a result, spontaneous emission of an atom in a cavity can be enhanced (inhibited spontaneous emission is also possible, but it is beyond the scope of this thesis). This effect was discovered by Edward M. Purcell in 1946 [15] and is referred to as the Purcell effect with the corresponding Purcell factor that characterizes the enhancement of the spontaneous emission. We will discuss the Purcell effect in the framework of cavity QED and derive a generalized Purcell factor. We will show that under certain conditions the generalized Purcell factor is reduced to the original Purcell factor proposed by Purcell.

1.3.1 Light-matter interaction

A cavity supports a number of discrete modes. Each mode has a specific resonance frequency, and field enhancement only occurs around the resonance frequency within a certain linewidth. For simplicity we study a single-mode cavity with a resonance frequency ω_c and a linewidth $\Delta\omega_c$ defined as the full width at half maximum (FWHM) of the cavity resonance. The quality factor Q_c of the cavity quantifies the number of field oscillations before the field leaks out of the cavity. It is defined as:

$$Q_c = \frac{\omega_c}{\Delta\omega_c} = \frac{\omega_c}{\kappa}, \tag{1.11}$$

where $\kappa \equiv \Delta\omega_c$ is the cavity decay rate. The quantized cavity field in analogy to the quantized field in a uniform medium as given by Eq. (1.8) reads ($N = 1$)

$$\boldsymbol{E}(\boldsymbol{r},t) = i\hat{\boldsymbol{e}}\sqrt{\frac{\hbar\omega_c}{2n_p n_g \epsilon_0 V}}\left(a\,u(\boldsymbol{r})e^{-i\omega_c t} - a^\dagger u^*(\boldsymbol{r})e^{i\omega_c t}\right), \tag{1.12}$$

where $u(\boldsymbol{r})$ is the transverse profile of the cavity mode. We expand the operator of the atomic dipole moment in the basis of the atom:

$$\begin{aligned}\boldsymbol{\mu} &= (|e\rangle\langle e| + |g\rangle\langle g|)\boldsymbol{\mu}(|e\rangle\langle e| + |g\rangle\langle g|)\\ &= |e\rangle\langle e|\boldsymbol{\mu}|g\rangle\langle g| + |g\rangle\langle g|\boldsymbol{\mu}|e\rangle\langle e|\\ &\equiv \vec{\mu}|e\rangle\langle g| + \vec{\mu}^*|g\rangle\langle e|\\ &\equiv \vec{\mu}\sigma_+ + \vec{\mu}^*\sigma_-,\end{aligned} \tag{1.13}$$

where we have defined $\vec{\mu} = \langle e|\boldsymbol{\mu}|g\rangle$, the atomic rising operator $\sigma_+ = |e\rangle\langle g|$, and the atomic lowering operator $\sigma_- = |g\rangle\langle e|$, while the terms $\langle e|\boldsymbol{\mu}|e\rangle$ and $\langle g|\boldsymbol{\mu}|g\rangle$ vanish since $\boldsymbol{\mu}$ has an odd parity.

With the expressions of $\boldsymbol{E}$ and $\boldsymbol{\mu}$, the interaction Hamiltonian as given by Eq. (1.3) can be rewritten as

$$\begin{aligned} H' &= -(\vec{\mu}\sigma_+ + \vec{\mu}^*\sigma_-)\cdot\left[i\hat{\boldsymbol{e}}\sqrt{\frac{\hbar\omega_c}{2n_p n_g \epsilon_0 V}}\left(a\,u(\boldsymbol{r})e^{-i\omega_c t} - a^\dagger u^*(\boldsymbol{r})e^{i\omega_c t}\right)\right] \\ &= -i\sqrt{\frac{\hbar\omega_c}{2n_p n_g \epsilon_0 V}}\Big[(\vec{\mu}\cdot\hat{\boldsymbol{e}})u(\boldsymbol{r})e^{-i\omega_c t}a\sigma_+ - (\vec{\mu}^*\cdot\hat{\boldsymbol{e}})u^*(\boldsymbol{r})e^{i\omega_c t}a^\dagger\sigma_- \\ &\quad +(\vec{\mu}^*\cdot\hat{\boldsymbol{e}})u(\boldsymbol{r})e^{-i\omega_c t}a\sigma_- - (\vec{\mu}\cdot\hat{\boldsymbol{e}})u^*(\boldsymbol{r})e^{i\omega_c t}a^\dagger\sigma_+\Big] \\ &= i\hbar g(a^\dagger\sigma_- e^{i\omega_c t} - a\sigma_+ e^{-i\omega_c t}), \end{aligned} \tag{1.14}$$

where we have omitted the terms with $a\sigma_-$ and $a^\dagger\sigma_+$ under the rotating wave approximation and defined a coupling constant g as

$$g = \sqrt{\frac{\omega_c}{2n_p n_g \hbar\epsilon_0 V}}(\vec{\mu}\cdot\hat{\boldsymbol{e}})u(\boldsymbol{r}) = \mu\sqrt{\frac{\omega_c}{2n_p n_g \hbar\epsilon_0 V}}|\cos\theta|u(\boldsymbol{r}), \tag{1.15}$$

with $\mu = |\vec{\mu}|$ and θ being the angle between the dipole moment and the local electric field.

1.3.2 Equations of motion

We are ready to write down the Hamiltonian of the atom-cavity system and to obtain equations of motion from the master equation. Depending on the coupling strength between the atom and the cavity field compared to decoherence rates of the system (such as atom dephasing rate, atom decay rate, and cavity field decay rate), two distinct regimes can be classified with different physics and phenomena. In the strong coupling regime in which the atom and the field exchange energy coherently with a rate that is faster than any decoherence rates, the system exhibits vacuum Rabi oscillation, vacuum Rabi splitting, and "collapse and revival" of the Rabi oscillation. On the other hand, in the weak coupling regime in which the coupling strength is smaller than one or more decoherence rates, the spontaneous emission rate of the atom can be modified by the cavity vacuum field that is different from the vacuum field in free space. The weak coupling regime is essential for efficient quantum information transfer between light and matter, and will be the regime explored in this thesis. We solve the equations of motion and obtain the expression for the generalized Purcell factor following the formalism as described in Ref. [16].

The Hamiltonian of the atom-cavity system can be written as

$$H = \hbar\omega_0\sigma_+\sigma_- + \hbar\omega_c a^+ a + i\hbar g(a^\dagger\sigma_- - a\sigma_+). \tag{1.16}$$

The master equation can be written as

$$\dot{\rho} = -\frac{i}{\hbar}[H,\rho] + \mathcal{L}_a\rho + \mathcal{L}_a^*\rho + \mathcal{L}_c\rho, \tag{1.17}$$

where $\mathcal{L}_a$, $\mathcal{L}_a^*$, and $\mathcal{L}_c$ are the Lindblad superoperators accounting for the decay of the atom, pure dephasing of the atom, and decay of the cavity field, respectively. Their explicit expressions are

$$\begin{aligned}
\mathcal{L}_a\rho &= \frac{\gamma}{2}(2\sigma_-\rho\sigma_+ - \sigma_+\sigma_-\rho - \rho\sigma_+\sigma_-),\\
\mathcal{L}_a^*\rho &= \frac{\gamma^*}{4}(2\sigma_z\rho\sigma_z - \sigma_z\sigma_z\rho - \rho\sigma_z\sigma_z),\\
\mathcal{L}_c\rho &= \frac{\kappa}{2}(2a\rho a^+ - a^+a\rho - \rho a^+a),
\end{aligned} \tag{1.18}$$

where κ is the cavity decay rate, γ is the atom decay rate, γ^* is the atom pure dephasing rate, and $\sigma_z = (|e\rangle\langle e| - |g\rangle\langle g|)/2$. We consider a system with only one excitation, i.e., the basis is truncated to $|e,0\rangle$ and $|g,1\rangle$. By multiplying operators of interest at both sides of the master equation and by taking traces, we obtain the equations of motion of their expectation values:

$$\begin{aligned}
\frac{\mathrm{d}\langle a^+a\rangle}{\mathrm{d}t} &= -\kappa\langle a^+a\rangle + g\langle\sigma_+a\rangle + g\langle a^+\sigma_-\rangle,\\
\frac{\mathrm{d}\langle\sigma_+\sigma_-\rangle}{\mathrm{d}t} &= -\gamma\langle\sigma_+\sigma_-\rangle - g\langle\sigma_+a\rangle - g\langle a^+\sigma_-\rangle,\\
\frac{\mathrm{d}\langle\sigma_+a\rangle}{\mathrm{d}t} &= -\left(\frac{\gamma}{2} + \frac{\kappa}{2} + \gamma^*\right)\langle\sigma_+a\rangle + g\langle\sigma_+\sigma_-\rangle - g\langle a^+a\rangle + i\Delta\langle\sigma_+a\rangle,
\end{aligned} \tag{1.19}$$

where $\langle X\rangle \equiv \mathrm{Tr}[\rho X]$ represents the expectation value of an operator X and $\Delta = \omega_a - \omega_c$ is the frequency detuning.

In the weak coupling regime, the coupling term $\langle\sigma_+a\rangle$ that is responsible for the Rabi oscillation can be adiabatically eliminated, i.e., $\mathrm{d}\langle\sigma_+a\rangle/\mathrm{d}t = 0$, but $\langle\sigma_+a\rangle \neq 0$. As a result, the equations of motion are simplified as

$$\begin{aligned}
\frac{\mathrm{d}\langle a^+a\rangle}{\mathrm{d}t} &= -(\kappa + R)\langle a^+a\rangle + R\langle\sigma_+\sigma_-\rangle,\\
\frac{\mathrm{d}\langle\sigma_+\sigma_-\rangle}{\mathrm{d}t} &= -(\gamma + R)\langle\sigma_+\sigma_-\rangle + R\langle a^+a\rangle,
\end{aligned} \tag{1.20}$$

where

$$R = \frac{2g^2\gamma_{\mathrm{tot}}}{\gamma_{\mathrm{tot}}^2 + \Delta^2}, \text{ with } \gamma_{\mathrm{tot}} = \frac{\gamma}{2} + \frac{\kappa}{2} + \gamma^*. \tag{1.21}$$

We notice that Eqs. (1.20) describe a coupled atom-cavity system exchanging energy with a rate R. The atom decays with a total rate of $\gamma + R$, while the cavity decays with a total rate of $\kappa + R$. Hence, the spontaneous emission rate of the atom is increased by R. The Purcell factor can be defined as

$$F = \frac{R}{\gamma} = \frac{2g^2\gamma_{\text{tot}}}{(\gamma_{\text{tot}}^2 + \Delta^2)\gamma}. \tag{1.22}$$

By using $g = \mu\sqrt{\frac{\omega}{2\hbar\epsilon V}}$ and $\gamma = \frac{\mu^2\omega^3 n}{3\pi\epsilon_0\hbar c^3}$, we obtain

$$F = \frac{3}{4\pi^2}\left(\frac{\lambda}{n_p}\right)^3 \frac{Q}{V}, \text{ with } Q = \frac{\omega_c\gamma_{\text{tot}}/2}{(\gamma_{\text{tot}}^2 + \Delta^2)}, \tag{1.23}$$

where λ is the wavelength in vacuum. Equation (1.23) is reduced to the well-known expression by Purcell for a zero detuning $\Delta = 0$ and when the cavity loss is the dominant decoherence process, i.e., $\kappa \gg \gamma, \gamma^*$ such that $\gamma_{\text{tot}} \approx \kappa/2$:

$$F = \frac{3}{4\pi^2}\left(\frac{\lambda}{n_p}\right)^3 \frac{Q_c}{V}. \tag{1.24}$$

1.4 Optical cavities

Equation (1.24) indicates that an optical cavity with a large quality factor Q_c and a small mode volume V is required to achieve a large Purcell factor. There are generally three types of optical cavities that have been intensively studied and optimized in terms of Q_c/V for the purpose of cavity QED experiments. In this section we shall summarize the properties of these cavities.

1.4.1 Ring resonators

A ring resonator is an optical device that guides light to travel in a closed cycle. It can be made of three or more mirrors reflecting light in a polygonal shape. This type of ring resonators is widely used as laser cavities. Light can also be guided by a waveguide structure in a circular shape (waveguide ring resonator) or by the boundary of a disk or a sphere with a higher refractive index than its surroundings (whispering-gallery mode (WGM) ring resonator). These two types of ring resonators are commonly used in cavity QED experiments.

Here we consider a general model in which a ring resonator is coupled to a straight waveguide via an evanescent field as shown in Fig. 1.1. Light in the ring resonator can travel in both clockwise and counter-clockwise directions. For simplicity we assume that the two travelling modes do not internally couple with each other and that the field propagating to the right (left) of the

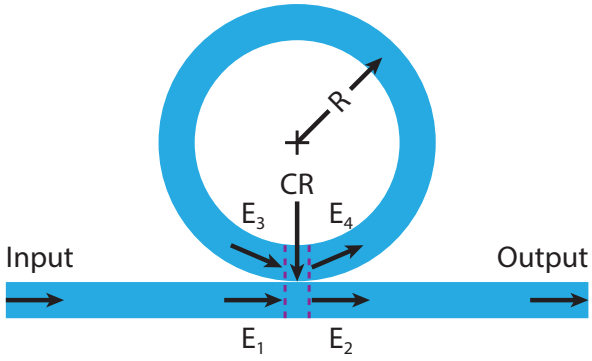

Figure 1.1: Schematic drawing of a single-mode waveguide coupled to a single-mode ring resonator via a coupling region (CR). Light is coupled into and out of the waveguide as denoted by the arrows. The electric fields at different positions are denoted by E_1–E_4. The radius of the ring resonator is R.

waveguide is only coupled to the counter-clockwise (clockwise) mode of the ring resonator and vice verse.

Based on the coupled mode theory [17], the four electric fields as defined in Fig. 1.1 are related by

$$E_2 = tE_1 + irE_3, \tag{1.25}$$
$$E_4 = irE_1 + tE_3, \tag{1.26}$$

where t and r are transmission and reflection coefficients, respectively. t and r are in general complex numbers, but they can be real if the coupling is phase-matched. Assuming the coupling is lossless, t and r satisfy

$$|t|^2 + |r|^2 = 1. \tag{1.27}$$

E_3 and E_4 are related by a phase shift and amplitude attenuation for one round trip in the ring resonator such as

$$E_3 = a\exp(i\phi)E_4, \tag{1.28}$$

where a and ϕ are electric field transmission and phase shift for one round trip in the ring resonator, respectively. a and ϕ are given by

$$a = \exp(-\alpha\pi R), \tag{1.29}$$
$$\phi = \frac{4\pi^2 R n_{\text{eff}}\,\nu}{c}, \tag{1.30}$$

where α is the intensity attenuation coefficient due to absorption, bending and scattering losses, n_{eff} is the effective refractive index of the mode of the

ring resonator, c is the speed of light in vacuum, ν is the frequency of the electromagnetic field, and R is the radius of the ring resonator. Substituting Eq. (1.28) into Eqs. (1.25) and (1.26) and solving the equations for E_1 and E_2, we obtain

$$\frac{E_2}{E_1} = \frac{r - a\exp(i\phi)}{1 - ra\exp(i\phi)}, \tag{1.31}$$

with the assistance of Eq. (1.27) and assuming that r and t are real numbers. The power transmission through the waveguide is therefore

$$T = \left|\frac{E_2}{E_1}\right|^2 = \frac{a^2 - 2ra\cos\phi + r^2}{1 - 2ra\cos\phi + r^2a^2}. \tag{1.32}$$

By examining Eq. (1.30), we find that the transmission as given by Eq. (1.32) is a periodic function of ν with the period or free spectral range (FSR)

$$\text{FSR} = \frac{c}{2\pi R n_{\text{eff}}}, \tag{1.33}$$

where we have ignored dispersion of the material for simplicity such that the phase index is equal to the group index. The resonance condition is given by $\cos\phi = 1$ and the resonance transmission is

$$T_0 = \frac{(a - r)^2}{(1 - ra)^2}. \tag{1.34}$$

We have $T_0 = 0$, if $a = r$ which is the critical coupling condition [18]. In the vicinity of resonance frequencies, $\cos\phi \approx 1 - \phi^2/2$ and Eq. (1.32) is approximately a Lorentzian function of ν. The linewidth of the resonance is

$$\Delta\nu = \frac{c(1 - ra)}{2\pi^2 R n_{\text{eff}}\sqrt{ra}}. \tag{1.35}$$

The quality factor is

$$Q = \frac{\nu}{\Delta\nu} = \frac{2\pi^2\nu R n_{\text{eff}}\sqrt{ra}}{c(1 - ra)}. \tag{1.36}$$

WGM ring resonators such as micro-toroids and micro-spheres are a special type of ring resonators that provides ultra-high quality factors. They are typically made of fused silica with a high purity. Light is confined close to the boundary of the ring resonator and therefore the surface smoothness is very critical for the quality factor. Atomic smoothness can be achieved by the surface tension of the material when melted. The quality factor of micro-toroids is typically on the order of 10^8 [19] and that of micro-spheres can be as high as 10^{10} [20]. A tapered optical fiber or a prism can be used to couple light in and out of the WGM ring resonators.

1.4.2 Fabry-Perot cavities

A Fabry-Perot cavity consists of two high-reflectivity mirrors facing each other. Light that matches the cavity modes bounces back and forth between the two mirrors before leaking out of the cavity. In practice usually concave mirrors are used to reduce the scattering due to the surface roughness of the mirrors. At resonance frequencies the forward- and backward-travelling light interfere constructively leading to a standing wave and an enhancement of the cavity field. The cavity field E_c in relation to the incident field E_i is given by

$$E_\mathrm{c} = \frac{\sqrt{1-R_1}}{1-e^{i\phi}\sqrt{R_1R_2}}E_\mathrm{i}, \tag{1.37}$$

where R_1 and R_2 are power reflectivity of the incident and output mirrors, respectively, ϕ is phase shift of the field after one-round trip, and we have ignored scattering and absorption losses. ϕ is given by

$$\phi = \frac{4\pi d\nu}{c}, \tag{1.38}$$

where d is the distance between the two mirrors, ν is the frequency of the field, and we have assumed the volume in between the two mirrors is vacuum with $n_p = 1$, but it is straightforward to extend to a material with $n_p \neq 1$. The output field is given by $E_\mathrm{o} = \sqrt{1-R_2}\,E_\mathrm{i}$ and therefore the transmission is

$$T = \left|\frac{E_\mathrm{o}}{E_\mathrm{i}}\right|^2 = \frac{(1-R_1)(1-R_2)}{1-2\cos\phi\sqrt{R_1R_2}+R_1R_2}. \tag{1.39}$$

The resonance condition is set by $\phi = 2\pi m$ with m being an integer. Therefore the resonance frequencies ν_0 are given by

$$\nu_0 = \frac{mc}{2d}. \tag{1.40}$$

On resonance, T is maximized and the resonance transmission T_0 reads

$$T_0 = \frac{(1-R_1)(1-R_2)}{(1-\sqrt{R_1R_2})^2}. \tag{1.41}$$

We have $T_0 = 1$ if $R_1 = R_2$, otherwise $T_0 < 1$. The quality factor is given by

$$Q = \frac{2\pi d\sqrt[4]{R_1R_2}}{\lambda(1-\sqrt{R_1R_2})}. \tag{1.42}$$

An important type of Fabry-Perot cavities with minimized mode volumes is a micro-pillar cavity. A micro-pillar cavity is a vertical cavity with its top and bottom mirrors made of distributed Bragg reflectors (DBR) separated by

a dielectric spacer. The DBR consists of alternating layers of two dielectric materials with different refractive indices. The thickness of each layer is one quarter of the wavelength in the material to have the maximum reflection. The cavity is etched in a pillar shape with a diameter of several micrometers. Figure 1.2(a) shows a scanning electron microscope (SEM) image of standard micro-pillar cavities. The sidewall of the pillar provides lateral confinement for the cavity modes and the scattering at the sidewall turns out to be the main source of cavity losses. The mode volume is typically smaller than ten times of a cubic wavelength in the material and the quality factor reaches up to 10^5.

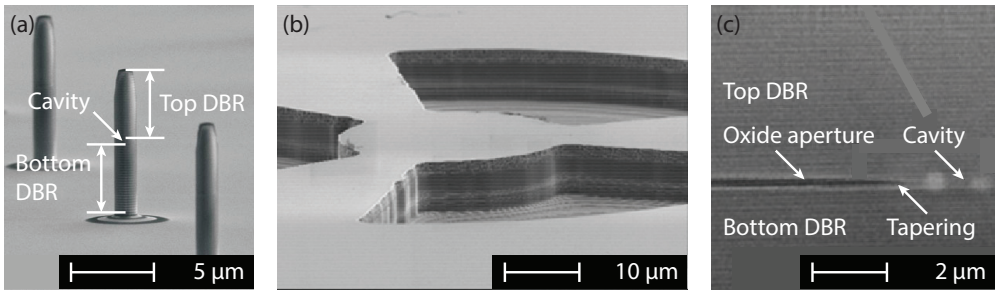

Figure 1.2: Scanning electron microscope (SEM) images of (a) three standard micro-pillar cavities, (b) an oxide-aperture micro-pillar cavity, and (c) a cross-section of the cavity as shown in (b). They are vertical Fabry-Perot cavities made of top and bottom distributed Bragg reflectors (DBR). In (a) the lateral confinement of light is achieved by the sidewall. (c) shows a tapered oxide aperture in the cavity as lateral confinement of light. (a) was obtained by the Department of Applied Physics at the University of Würzburg. (b) and (c) are adopted from Ref. [21].

A more advanced and complicated version of the micro-pillar cavity is an oxide-aperture micro-pillar cavity. There is an aluminium-concentrated layer between the two DBRs. The cavity is etched down to a larger diameter (tens of micrometers) compared with the standard micro-pillar cavity. A SEM image of an oxide-aperture micro-pillar cavity is shown in Fig. 1.2(b) and its cross-section is shown in Fig. 1.2(c). There are unetched bridges connecting the micro-pillar to the surroundings which strengthen the structure and enable electrical connections to the cavity. The aluminium-concentrated layer is then oxidized through the etched trenches to form a tapered aperture at the cavity region as shown in Fig. 1.2(c). This oxide aperture provides lateral confinement of the cavity modes. Compared with the standard micro-pillar cavity, the oxide-aperture micro-pillar cavity typically has a higher quality factor because the tapered oxide aperture induces less light scattering than the sidewall of the standard micro-pillar cavity. Furthermore, it is also much more mechanically stable and capable of applying electrical connections to the cavity, e.g., quantum dots in a p-i-n junction in the cavity can be tuned by an

applied voltage. We have succeeded in making permanent optical fiber connections to the oxide-aperture micro-pillar cavities which can be used at cryogenic temperatures. This will be presented in Chapter 3 of this thesis.

1.4.3 Photonic crystal cavities

Photonic crystals are artificial dielectric materials consisting of periodic scatterers for electromagnetic waves in analogy to real crystals where atoms form a periodic lattice scattering electrons. Because of the periodic scattering, photonic band structures emerge in the energy/frequency domain similar with the energy bands in real crystals. Electromagnetic modes are allowed in certain bands only and forbidden in "band gaps". If one or several local scatterers are removed from the photonic crystal as a defect, the band structures will be modified locally around the defect site. Consequently, in a band gap, electromagnetic modes are allowed to exist nowhere but only around the defect, which effectively creates confinement or a cavity for the electromagnetic field.

A photonic crystal can be of different dimensions, e.g., a DBR can be viewed as a one-dimensional photonic crystal, but in this introductory section we limit our discussions only to two-dimensional (2D) cases. A 2D photonic crystal cavity is made of a dielectric slab with a refractive index higher than its surroundings (typically air). Electromagnetic fields are confined in the slab by total internal reflection. Periodic scatterers are created as etched holes in the slab with their diameters comparable with the wavelength of the field. The positions of the holes are determined by numerically solving Maxwell's equations for the target wavelength. One or several holes are unetched to modify the local photonic density of states. The mode volume is approximately a cubic wavelength in the material and the quality factor is typically on the order of 10^4.

1.5 Rare-earth ions in solids

Generally speaking, rare-earth elements are 17 chemical elements in the periodic table including 15 lanthanides from lanthanum (La, atomic number 57) to lutetium (Lu, 71) plus scandium (Sc, 21) and yttrium (Y, 39). Concerning optical properties and applications in solids, only 13 elements from cerium (Ce, 58) to ytterbium (Yb, 70) are important and throughout this thesis the term "rare-earth" will be only referred to as these 13 elements. The rare-earth elements share similar electronic configurations as shown in Figs. 1.3(a) and 1.3(b): a core with the electronic configuration of xenon (Xe, 54) , $4f^n$ orbit, and $6s^2$ orbit (for Ce there is an additional $5d^1$ orbit), where the numbers before the letters are principal quantum numbers, the letters denote angular

momentum quantum numbers: $s = 0,\ p = 1,\ d = 2,\ f = 3, \cdots$, and the superscripts are the numbers of electrons in the particular orbits. The number of electrons in the $4f$ orbit n ranges from 1 for Ce to 14 for Yb. A special aspect of rare-earth elements with important implications is that the $4f$ orbit is spatially enclosed within the filled $5s$ and $5p$ orbits in the Xe shell, a phenomenon called "lanthanide contraction", which effectively shields the $4f$ orbit from the environment. Calculated radial probabilities of $4f$, $5s$, and $5p$ orbits of Yb are shown in Fig. 1.4 as an example to illustrate the lanthanide contraction.

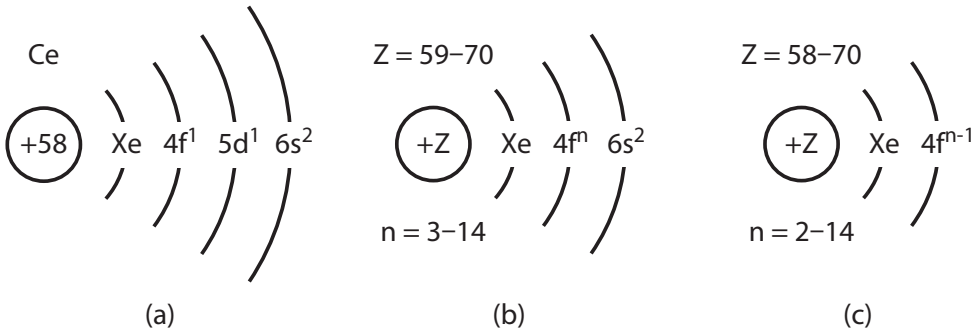

Figure 1.3: Electronic configurations of (a) cerium (Ce, atomic number 58) atom, (b) other rare-earth atoms, and (c) trivalent rare-earth ions. The inner xenon (Xe, 54) shell has a configuration of $1s^2 2s^2 2p^6 3s^2 3p^6 3d^{10} 4s^2 4p^6 4d^{10} 5s^2 5p^6$. In these notations the letters denote angular momentum quantum numbers: $s = 0,\ p = 1,\ d = 2,\ f = 3, \cdots$, the numbers before the letters are principal quantum numbers, and the superscripts are the numbers of electrons in the particular orbits. For ytterbium (Yb, 70), $n = 14$.

Rare-earth elements can be doped in solids such as glass and inorganic crystals to form trivalent ions by losing two electrons from the $6s$ orbit and one electron from the $4f$ orbit (for Ce it loses two electrons from the $6s$ orbit and one electron from the $5d$ orbit). The resulting electronic configurations of the trivalent ions are a Xe shell and the $4f$ orbit as shown in Fig. 1.3(c). The number of electrons on the $4f$ orbit ranges from 1 for Ce^{3+} to 13 for Yb^{3+}. Since the maximum number of electrons that can occupy the $4f$ orbit is 14, it can be considered as a single hole for Yb^{3+}. In principal dipole transitions within the $4f$ states of an isolated rare-earth ion are forbidden because the initial state and the final state have the same parity. However, interactions with the lattice field in the host material admix higher-lying states with opposite parity into the $4f$ states. As a result, dipole transitions within the $4f$ states become partially allowed, although these transitions are still extremely weak (small dipole moments) compared with fully allowed dipole transitions. The energy diagrams of the $4f$ states are typically very complex with exceptions for Ce^{3+} and Yb^{3+} for which only one electron or one hole is in the $4f$ states. For instance for Yb^{3+} there are simply two energy levels with three double-

degenerate manifolds on the excited state and four double-degenerate manifolds on the ground state as shown in the inset of Fig. 1.4. The spectra of the $4f$ transitions are within the range of visible and infrared and exhibit sharp peaks even at room temperature essentially because of the shielding of the $4f$ orbit by the outer filled $5s$ and $5p$ orbits. Due to the small dipole moment, the radiative lifetimes of the $4f$ states are typically on the order of milliseconds.

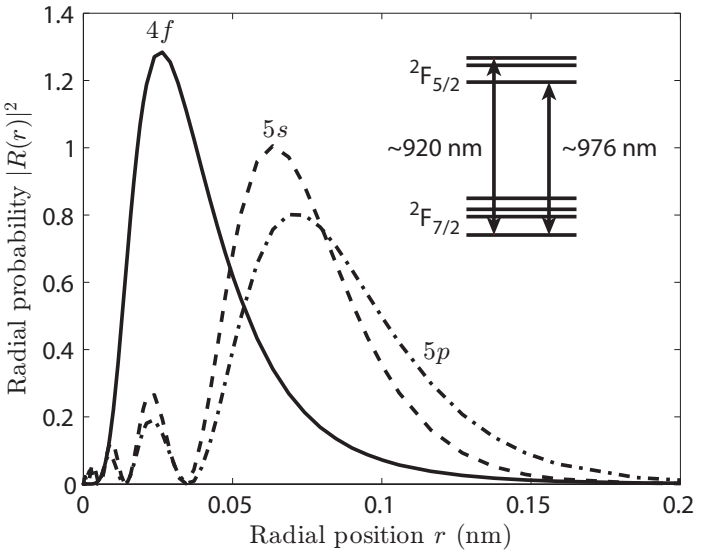

Figure 1.4: Radial probabilities of $4f$ (solid curve), $5s$ (dashed curve), and $5p$ (dash-dot curve) electronic orbits of ytterbium (Yb) atoms as a function of radial position. The data are adopted from Ref. [22] resulting from numerical calculations based on the Hartree-Fock method. The $4f$ orbit is largely enclosed in the filled $5s$ and $5p$ orbits. Inset: energy level diagram of the $4f$ electrons of Yb^{3+} in silicon dioxide. There are four manifolds (stark sub-levels) at the ground state and three manifolds at the excited state. The transitions between the ground state and the excited state involve near-infrared photons.

Rare-earth-doped solids have found many important applications for lasers and optical communications. Rare-earth-doped glass and crystals, especially neodymium (Nd, 60)-doped yttrium aluminum garnet (YAG) are the foundation of modern solid-state lasers with much higher stability, efficiency, tunability, and power capability than gas lasers. Erbium (Er, 68)- and Yb-doped optical fibers are widely used as gain media of fiber lasers and as amplifiers for optical communications. Recently, rare-earth ions in crystals attract new interests for quantum information applications because of the high quantum coherence of the $4f$ states at low temperature [23]. In the past few years, collective effects of ensembles of rare-earth ions have been used as quantum memories for single photons [5, 6] and quantum entanglement of two remote crystals [24]

has been experimentally demonstrated. Single rare-earth ions in crystals were very recently detected by using different advanced techniques [25, 9, 7, 8]. They show the great potential of rare-earth ions for future quantum information applications and form the basic motivation to study cavity QED with rare-earth ions. This thesis presents results of solid-state rare-earth cavity QED with, up to now, only a few preliminary studies [26, 27, 28, 29, 30, 31].